Journal Name

ARTICLE TYPE

Cite this: DOI: 00.0000/xxxxxxxxxx

Disordered wax platelets on Tradescantia pallida leaves create golden shine†

Gea T. van de Kerkhof,[a‡] Lukas Schertel,[a‡] Rebecca Poon,[a] Gianni Jacucci,[a] Beverley J. Glover,[b] and Silvia Vignolini*[a]

Received Date
Accepted Date

DOI: 00.0000/xxxxxxxxxx

Plants have various strategies to protect themselves from harmful light. An example of such a protective mechanism is the growth of epicuticular nanostructures, such as a layer of hair or wax crystals. Most nanostructures are optimised to screen UV radiation, as UV light is particularly damaging for cellular tissue. We find that, contrary to the commonly found UV reflectance, the epicuticular wax crystals on *Tradescantia* leaves reflect strongly in the higher visible wavelength regime. Thus, they give the leaves a golden shine. We characterize the optical appearance of *Tradescantia pallida* 'purpurea' leaves by angularly resolved spectroscopy and compare the results to finite difference time domain simulations. We find that it is the disordered assembly of the wax platelets that is the crucial parameter to obtain the observed reflected intensity increase for higher wavelengths.

1 Introduction

Plants have developed a wide variety of strategies to manipulate light for different functions: (i) to harness energy from light via photosynthesis, by redirecting light into their photosynthetic organs [1–3], (ii) for inter-species communication, optimising their appearance and colouration via light interaction with pigments [4,5], or with photonic structures [6], (iii) for photoprotection: to protect their cellular tissue from an excess of radiation [7]. Photoprotection is achieved in different ways: by adapting mesophyll thickness and composition [8,9], by growing highly reflective nanostructures [10–14], or simply by growing protective structures in the epidermis such as hair (pubescent) [15–19] and an increase in the production of wax (glaucous) [20–22].

While an increased mesophyll thickness provides photoprotection by decreasing light power density (i.e. redistributing the light intensity in the tissue), reflective nanostructures backscatter part of the radiation, thereby impeding penetration in deeper tissue and decreasing power density for the forward propagating light. The presence of these wax crystals and hairs can immediately be recognised in leaves as they provide the tissue with a pearlescent white or blue appearance [23]. In general, as the most high-energy solar radiation is in the UV range, the shape and composition of waxes are optimised to either absorb or efficiently reflect this spectral region [24].

Tradescantia pallida 'purpurea' has been reported to exploit several photoprotective mechanisms: upon exposure to high light intensity it changes its pigment content and tissue anatomy, increasing the mesophyll thickness [25–27], and it grows an epicuticular layer of wax platelets [25]. Surprisingly, contrary to the commonly observed short wavelength reflectance, the wax platelets produced in the cuticular layer provide the leaves of *Tradescantia* with increased reflectance at larger wavelengths. Such increased reflectance above 500 nm provides a golden appearance to the leaves, which can be observed only at specific angles along the specular reflection direction, posing the question of its biological significance. This stands in sharp contrast to the diffuse light scattering commonly observed from wax crystals.

Here, we characterise the optical response of the leaves and compare it with their anatomy, by combining angularly resolved spectroscopy with scanning electron microscopy (SEM) and optical imaging. We show that the wax scatters light at specular reflection more strongly for larger wavelengths and we use finite difference time domain calculations to show that the origin of this high wavelength increase lies in the behaviour of the wax platelets as disordered scatterers.

2 Methods

2.1 Sample preparation

Leaves from *Tradescantia pallida* 'purpurea' were collected from Cambridge University Botanic Garden. Samples were measured fresh in multiple configurations: (1) entire tissue, (2) cell wall of

[a] *University of Cambridge, Department of Chemistry, Lensfield Road, Cambridge, CB2 1EW, The United Kingdom.*
[b] *University of Cambridge, Department of Plant Sciences, Downing Street, CB2 3EA, Cambridge, The United Kingdom.*

† Electronic Supplementary Information (ESI) available. See DOI: 00.0000/00000000.

‡ These authors contributed equally to this work.

the outer cells in the epidermis with wax only and (3) epidermal cell wall with no wax. For configuration (2) and (3) the underlying pigmented tissue layers were removed from the abaxial side of the leaves with a scalpel, leaving only the transparent adaxial cell walls of the outer epidermal cells and the cuticle with epicuticular wax (Figure S1a†), to better isolate the optical response of the wax from the underlying layers of the leaf. For removal of the wax layer in (3), epidermal samples were additionally rubbed manually and rinsed with ethanol.

2.2 Scanning Electron Microscopy

SEM imaging was performed on a TESCAN MIRA3 FEG-SEM system. Samples were sputter coated with Pt (10 nm) prior to measurements (Quorum Technologies Q150T ES). For cross section imaging the leaves were freeze fractured by immersion in liquid nitrogen.

2.3 Angularly resolved spectrometry

Angularly resolved spectra were taken using a custom-built goniometer setup (Figure S1†, Vignolini et al[4]). Collimated light in the UV-VIS region with a spot size of 5 mm diameter (Ocean Optics HPX-2000 xenon lamp) was directed onto the sample, which was mounted on a rotating stage so that the angle of incident light could be varied. Light that is reflected and scattered from the sample is collected by an optical fiber connected to a spectrometer (AvaSpec-HS2048, Avantes). The detection fiber is connected to a rotating arm so that the angle of detection can be varied. At the detection angle which equals the negative of the incident anglered, no signal is collected due to a limitation in the setup. All the spectra reported in the paper are normalised against a white diffuser (labsphere SRS-99-010).

2.4 Finite difference time domain simulations

The numerical calcualtions were performed using LUMERICAL 8.22 (Lumerical Solutions Inc., Vancouver, BC, Canada), a commercial software based on the finite difference time domain method. In a first step the single scattering properties of wax platelets were investigated. A cuboid scatterer with dimensions 1μm x 50 nm x 1μm, as extracted from SEM images, was created and the scattering efficiency was measured in response to a plane incident wave. The scattering efficiency is defined as the ratio between the scattering cross section and the geometrical cross section of a particle. In detail, the scattering cross section was calculated as the ratio between the power of the incident source and the scattered radiation while the geometrical cross section is defined as the area of the particle in the direction perpendicular to the incoming beam. In the simulations, both the dimensions of the scatterer and the incident angle were varied independently (Figure 3).

2D simulations of wax platelets on top of a fixed layer were also performed. The layer was set to a thickness of $d = 2.3$ μm (extracted from SEM images of the cell wall of the outer cells in the epidermis) with a refractive index of $n = 1.4$ (see section 2.5). Rectangle shaped platelets of width 50 nm and height 1μm were placed on top of the layer. In a second step they were tilted by angle θ normally random distributed with mean 0° and standard deviation of 20°. Both total and specular reflection were measured first for the flat layer only, then for the layer with platelets and finally for the layer with disordered tilted platelets. An average over 10 thicknesses between 0.5μm to 2.3μm (as extracted from SEM) was performed in a last step.

2.5 Refractive index determination

The approximate refractive index value of the wax was determined by index matching isolated wax platelets (Figure S5a-c†). These were collected on a microscope slide and imaged with a Zeiss Axio Microscope. Refractive index matching oils (Cargille series A) of $n = 1.50$ to $n = 1.55$ were added to the wax to observe at which value of n the wax apparently disappeared.

Similarly, the approximate refractive index value of the underlying substrate was determined by measuring the specular reflectance for an average of four samples (all in configuration 3) in the 400 to 800 nm range, using an integrating sphere (Labsphere) illuminating at angle 10° (Figure S5d†). Samples were illuminated using a Xenon lamp Ocean Optics HPX-2000 coupled into an optical fiber. Reflected light was detected using a spectrometer (AvaSpec-HS2048, Avantes). The results of these measurements were compared with calculations of the refractive index using the Fresnel equation for normal incidence, assuming that the reflectance is effectively constant over the range 0° - 10°.

3 Results and Discussion

3.1 Wax platelets give a golden shine

Leaves of *Tradescantia pallida* 'purpurea' have a golden appearance under direct illumination (Figure 1a). This colour disappears after mechanical removal of its epicuticular wax layer, leaving only a reflection of white light. Therefore, we find that the golden appearance of the leaf is inherent to the presence of the wax.

Studying the cuticle of *Tradescantia* leaves with SEM shows that this wax layer appears as a collection of platelets (Figure 1b). Samples where the wax layer is still present, but smudged into a flat layer rather than a collection of platelets, no longer exhibit the golden appearance (Figure S2†). This indicates the importance of the platelet morphology and organisation for obtaining this optical effect. Samples which have undergone mechanical removal of the wax show a flat, featureless cuticle, which gives off a white reflectance.

3.2 Long wavelength increase at specular reflection

To characterise the golden appearance of the leaf, we used angularly resolved spectrometry on the isolated epidermal cell wall layer with epicuticular wax (configuration 2, see section 2.1). We observe that for a range of incident light angles, between 5° and 60°, the long wavelength spectral region has high reflectivity at the specular reflection direction (Figure 2, S4†). In contrast, for samples with the wax layer removed (configuration 3, see section 2.1) we observe that the spectrum is almost flat, with a slight increase in the UV, corresponding to the white reflection observed in the epi-illumination microscopic picture in Figure 1.

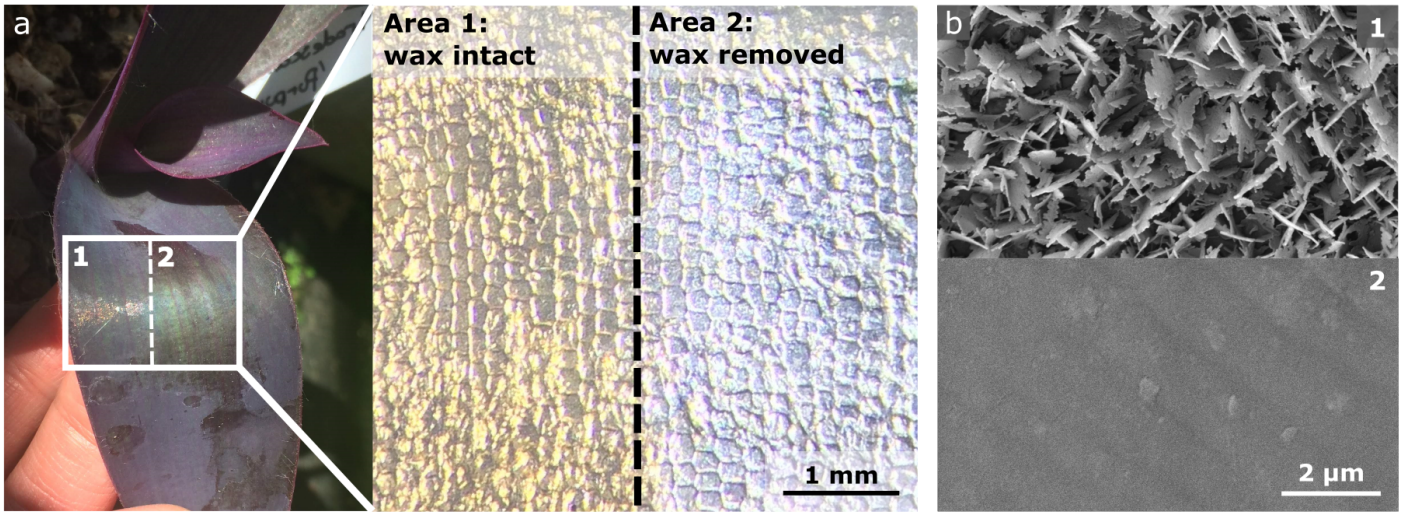

Fig. 1 a) A leaf of *Tradescantia pallida* 'purpurea', photograph of the entire leaf and corresponding microscope pictures. 1 and 2 represent the areas of interest. In area 1 the wax layer is intact, giving a golden reflection. In area 2 the wax layer is removed, giving a more specular signal under direct illumination (2). b) SEM top view images of the leaf cuticle with and without wax, corresponding to areas 1 and 2 in (a), respectively.

The enhanced reflectivity at larger wavelengths, present only in the specular direction, shows a directional scattering contribution of the wax crystals, as a wavelength selective absorbance of the wax would appear angularly independant and not increase the scattering above 500 nm.

3.3 Origin of the long wavelength increase

To identify the physical origin of the golden colour, we investigated the effect of the morphology of the wax layer using finite difference time domain (FDTD) calculations. Wax crystals are known to have the ability to influence the scattering properties of leaves[28]. Therefore, we first investigated the behaviour of the wax platelets as single scatterers (Figure 3a). We then continued to consider the effect of adding the platelets together in a two dimensional film.

The parameters used in the simulations are obtained from the SEM images (Figure 4a), and the values of the refractive indices of the wax and the substrate are obtained from the refractive index matching experiments (Figure S5†). The platelets are irregular in shape, with an approximate long axis of length 1 μm and an approximate width of 50 nm. The thickness of the substrate is considered to vary between 0.5 and 2.3 μm, while the refractive index of the wax is set to 1.52 $\pm$0.01, and the average refractive index of the epidermal cell wall is set to be 1.42 $\pm$0.02.

In the numerical calculations, we observe that, regardless of the dimensions of the platelets and the angle of incident light, a single platelet does not scatter light more strongly for higher visible wavelength regions than for lower ones (Figure 3b-d). Instead, fringes from thin film effects appear to provide a slight increase of scattering efficiency in the low wavelength region for some configurations.

Thus, as the single scattering of the platelets is not accountable for the observed behaviour, we investigate the scattering behaviour of a two-dimensional collection of platelets on a substrate (Figure 4).

We first considered the optical response of the substrate only. For a bare substrate, with no wax, we obtain a spectrum that oscillates evenly across the wavelength range, without an increase at any particular wavelength (Figure 4b, black line). This shows that an isolated layer of cell walls of homogeneous thickness acts as a thin film. Adding a layer of ordered platelets to this substrate leads to a similar spectral behaviour (Figure 4b, light blue line). Introducing orientational disorder to the platelets gives a fringed spectrum with an intensity increase at higher wavelengths in specular reflection (Figure 4b, yellow line). Note that such intensity increase at long wavelength is only found in the specular reflection direction, and not when measuring total reflection, where the signal gets obscured by high intensity reflection at other angles (Figure S6†). A similar result is obtained when defining the cuticle as a substrate with rough surface instead of having disordered platelets on top of a flat surface (Figure S7a†). Such results highlight that the disorder in orientation and position of the platelets is the crucial parameter giving rise to the golden reflection.

In the experimental spectra a continuous long wavelength increase of the reflection, with only small oscillations, was observed (Figure 2b, S4†). In contrast, the simulations show large fringes with an on average intensity increase in the long wavelength region. Previous work shows that a similar difference can be found when comparing thin film reflection spectra for films with a fixed thickness to films of varying thickness[29]. Averaging of a range of film thicknesses reduces the amplitude of the oscillations in the reflection spectra[30]. Indeed, when we switch from the fixed underlying substrate thickness used in Figure 4b to an average of a set of reflection curves for different substrate thicknesses (Figure 4c, S7b†), the amplitude of the oscillations reduces significantly. We find a reflection curve of a similar shape as observed in the experiments (Figure 2), showing a continuous intensity increase in the long wavelength region. This approach can be further justified when looking at SEM images (S8†), where a large local vari-

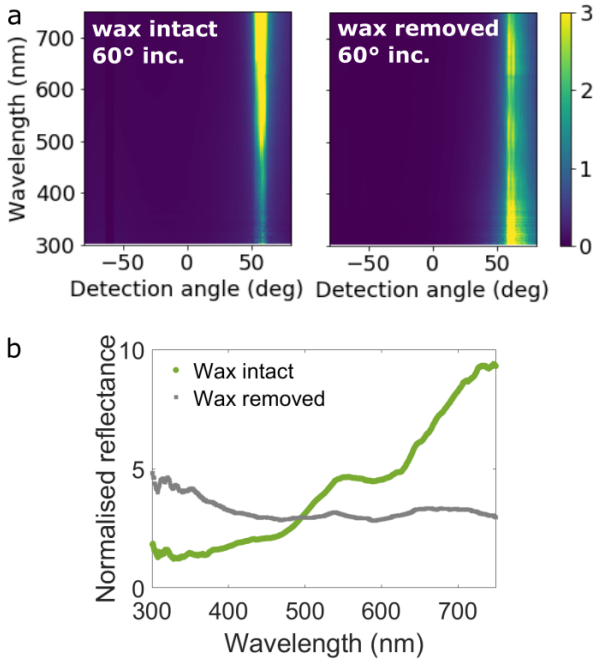

Fig. 2 a) Angularly resolved scattering plot for epidermal cell wall with and without wax platelets illuminated at a fixed angle of incidence (60°). Light intensity is represented on a blue to yellow colour scale, constant for both plots, displaying the reflectance intensity normalised against a white diffuser. The specular reflection of leaves with an intact wax layer shows an increase in intensity for higher wavelengths. The specular reflection of leaves with wax removed show a constant intensity for the specular signal at all visible wavelengths. b) Single angle spectra taken from (a) at highest intensity of reflection: specular reflection ±2°. Angular deviation from specular angle lies within error range of goniometer setup.

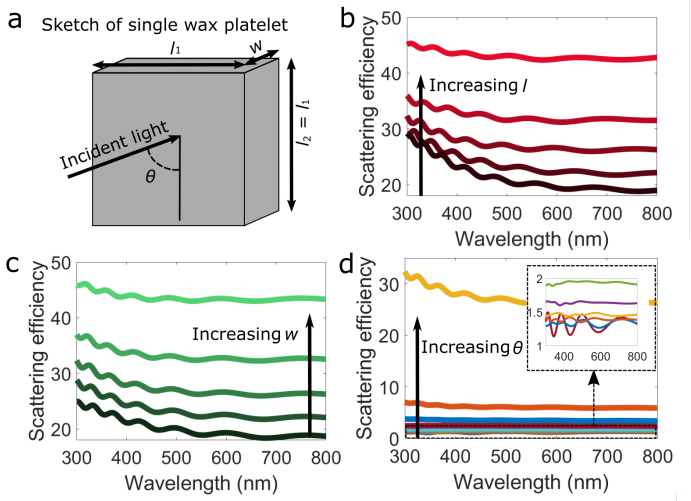

Fig. 3 a) Sketch of a wax platelet as a single scatterer, showing all its relevant dimensions. l is the length of the platelet, where $l_1 = l_2$. w is the width, and θ the angle of light incident on the platelet. b), c) and d) show FDTD simulations of the scattering efficiency for platelets with varying l, w and θ, respectively. Length varies from 0.6 to 1.4 μm, with stepsize 0.2 μm, width varies from 30 to 70 nm, with stepsize 10 nm, and θ varies from 0° to 90°, with stepsize 10°. When changing a parameter value, the other values were kept constant at $l = 1$ μm, $w = 50$ nm and $\theta = 90°$.

ation in the substrate thickness is observed. As the experimental spectra in Figure 2 are an average reflectance over a large sample area (20 mm^2), they will represent an average of many different substrate thicknesses.

3.4 Biological function of the golden appearance

While we were able to disentangle the physical origin of the colouration, its biological function remains to be determined. Whereas the optical properties of wax are often used by plants for photoprotection, the limited angular visibility of the red wavelength increase makes this an unlikely explanation in this case.

We speculate that a possible function of the golden appearance is to repel herbivores. Red colours are often a signal of lower nutrient content in leaves: anthocyanic margins in leaves are induced in response to mineral deficiencies[31], and leaves turn red in autumn shortly before dying off. Therefore, herbivores tend to avoid them[32]. Red is also often used by plants as aposematic colouration[33]. *Tradescantia* produces anthocyanins that could function for aposematism as well, but it only has the colour on its abaxial side, presumably because adaxial anthocyanins would interfere with photosynthesis[34].

Another possibility is that the wax platelets serve a different function, unrelated to the optical response. Epicuticular waxes are known to have a range of functions[35,36]. Even without the here described long wavelength reflection, wax crystals can act to repel herbivores: Waxy surfaces can impede insect attachment[37], or the epicuticular waxes can obscure feeding stimulants that are present in the leaf[38]. In addition to this, epicuticular wax can also create hydrophobic surfaces that function to cleanse the leaves from pathogens and other particles[39–41]. *Tradescantia* leaves are para-hydrophobic[42], meaning that by combining epicuticular and surface roughness they can efficiently collect water droplets for self-irrigation in arid environments[43]. This gives the plant an adaptive advantage that allows it to survive in a larger range of environments.

4 Conclusions

In conclusion, we studied the optical response of epicuticular wax crystals on the leaves of *Tradescantia pallida purpurea*. We report a golden appearance of the leaves under direct illumination, which disappears upon removal of the layer of wax platelets. Characterisation of this golden colour shows a gradual increase in specular reflection intensity for higher visible wavelengths. FDTD simulations show that this long wavelength increase originates from the disordered arrangement of the wax platelets on a substrate, where the platelets act as light scatterers. We show that the orientational disorder is the crucial parameter for obtaining the long wavelength increase.

Given its long wavelength response, it is unlikely that the usual function of wax crystals on these leaves is in photoprotection, opening interesting questions about its actual biological function.

Conflicts of interest

There are no conflicts to declare.

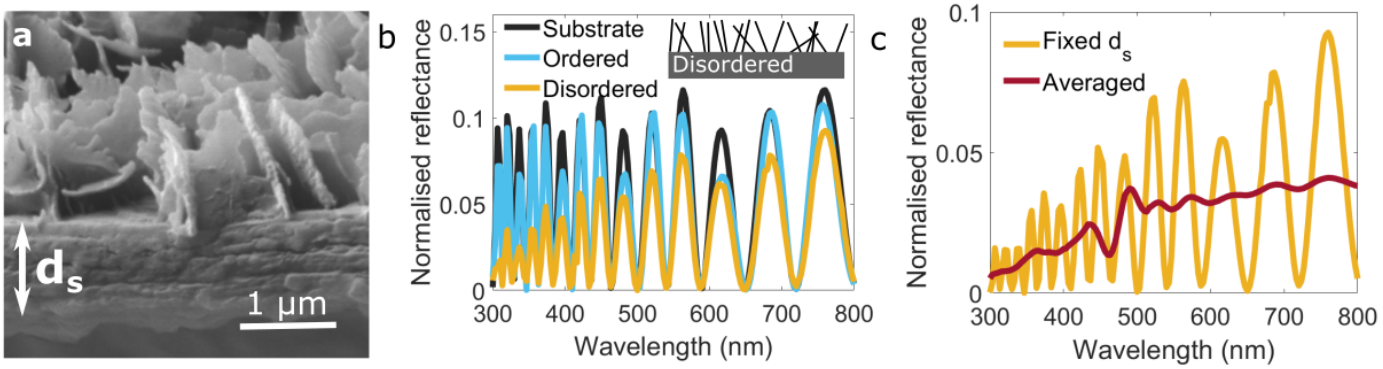

Fig. 4 a) Cross-sectional SEM of a leaf, displaying the epicuticular wax platelets on the epidermis, used to determine platelet and substrate dimensions. b) FDTD simulation of leaf reflectance at specular angle. Reflectance of the substrate at fixed thickness, with and without ordered platelets, shows thin film behaviour. Addition of disorder to the platelet orientation yields the experimentally observed long wavelength increase. c) Averaging of a set of spectra obtained by FDTD simulations of varied substrate thicknesses removes the fringes.

Acknowledgements

This work was funded by by EU's Horizon 2020 research and innovation programme under the Marie Skłodowska-Curie grant agreement No. 722842 (ITN Plant-inspired Materials and Surfaces–PlaMatSu), the Swiss National Science Foundation under project P2ZHP2_183998 and BBSRC David Phillips Fellowship (BB/K014617/1) and the European Research Council (ERC-2014-STG H2020 639088).

Notes and references

1 T. C. Vogelmann, *Annual review of plant biology*, 1993, **44**, 231–251.
2 K. K. Niyogi, *Annual review of plant biology*, 1999, **50**, 333–359.
3 M. Jacobs, M. Lopez-Garcia, O.-P. Phrathep, T. Lawson, R. Oulton and H. M. Whitney, *Nature plants*, 2016, **2**, 16162.
4 S. Vignolini, E. Moyroud, B. J. Glover and U. Steiner, *Journal of The Royal Society Interface*, 2013, **10**, 20130394.
5 B. D. Wilts, P. J. Rudall, E. Moyroud, T. Gregory, Y. Ogawa, S. Vignolini, U. Steiner and B. J. Glover, *New Phytologist*, 2018, **219**, 1124–1133.
6 E. Moyroud, T. Wenzel, R. Middleton, P. J. Rudall, H. Banks, A. Reed, G. Mellers, P. Killoran, M. M. Westwood, U. Steiner *et al.*, *Nature*, 2017, **550**, 469–474.
7 M. A. Jansen, V. Gaba and B. M. Greenberg, *Trends in plant science*, 1998, **3**, 131–135.
8 T. Vogelmann and G. Martin, *Plant, Cell & Environment*, 1993, **16**, 65–72.
9 K. S. Gould, D. N. Kuhn, D. W. Lee and S. F. Oberbauer, *Nature*, 1995, **378**, 241.
10 C. Hébant and D. W. Lee, *American Journal of Botany*, 1984, **71**, 216–219.
11 D. W. Lee, *Nature*, 1991, **349**, 260.
12 B. J. Glover and H. M. Whitney, *Annals of botany*, 2010, **105**, 505–511.
13 D. W. Lee, Biomimetics and Bioinspiration, 2009, p. 740104.
14 K. S. Gould and D. W. Lee, *American Journal of Botany*, 1996, **83**, 45–50.
15 G. Karabourniotis, K. Papadopoulos, M. Papamarkou and Y. Manetas, *Physiologia Plantarum*, 1992, **86**, 414–418.
16 Y. Manetas, *New Phytologist*, 2003, **158**, 503–508.
17 A. Yan, J. Pan, L. An, Y. Gan and H. Feng, *Journal of Photochemistry and Photobiology B: Biology*, 2012, **113**, 29–35.
18 J. Ehleringer, O. Björkman and H. A. Mooney, *Science*, 1976, **192**, 376–377.
19 M. Holmes and D. Keiller, *Plant, Cell & Environment*, 2002, **25**, 85–93.
20 R. Grant, M. Jenks, P. Rich, P. Peters and E. Ashworth, *Agricultural and Forest Meteorology*, 1995, **75**, 263–281.
21 L. M. Long, H. P. Patel, W. C. Cory and A. E. Stapleton, *Functional plant biology*, 2003, **30**, 75–81.
22 J. P. Vigneron, M. Rassart, Z. Vértesy, K. Kertész, M. Sarrazin, L. P. Biró, D. Ertz and V. Lousse, *Physical review E*, 2005, **71**, 011906.
23 J. B. Clark and G. R. Lister, *Plant physiology*, 1975, **55**, 407–413.
24 T. W. Mulroy, *Oecologia*, 1979, **38**, 349–357.
25 É. A. S. Paiva, R. M. d. S. Isaias, F. H. A. Vale and C. G. d. S. Queiroz, *Brazilian Archives of Biology and Technology*, 2003, **46**, 617–624.
26 D. Dewez and F. Perreault, *Acta physiologiae plantarum*, 2013, **35**, 463–472.
27 A. J. Young, *Physiologia Plantarum*, 1991, **83**, 702–708.
28 T. W. Brakke, W. P. Wergin, E. F. Erbe and J. M. Harnden, *Remote sensing of Environment*, 1993, **43**, 115–130.
29 D. G. Stavenga, *Materials Today: Proceedings*, 2014, **1**, 109–121.
30 D. G. Stavenga, J. Tinbergen, H. L. Leertouwer and B. D. Wilts, *Journal of Experimental Biology*, 2011, **214**, 3960–3967.
31 J. T. Raese, *Communications in soil science and plant analysis*, 2002, **33**, 461–477.

32 T. F. Döring, M. Archetti and J. Hardie, *Proceedings of the Royal Society B: Biological Sciences*, 2008, **276**, 121–127.
33 L. J. Cooney, J. W. Van Klink, N. M. Hughes, N. B. Perry, H. M. Schaefer, I. J. Menzies and K. S. Gould, *New Phytologist*, 2012, **194**, 488–497.
34 W. Steyn, S. Wand, D. Holcroft and G. Jacobs, *New Phytologist*, 2002, **155**, 349–361.
35 M. Riederer and C. Muller, *Annual Plant Reviews, Biology of the Plant Cuticle*, John Wiley & Sons, 2008, vol. 23.
36 C. Müller and M. Riederer, *Journal of chemical ecology*, 2005, **31**, 2621–2651.
37 S. Eigenbrode, T. Castagnola, M.-B. Roux and L. Steljes, *Entomologia Experimentalis et Applicata*, 1996, **81**, 335–343.
38 K. Reifenrath, M. Riederer and C. Müller, *Entomologia Experimentalis et Applicata*, 2005, **115**, 41–50.
39 W. Barthlott and C. Neinhuis, *Planta*, 1997, **202**, 1–8.
40 K. Koch and H.-J. Ensikat, *Micron*, 2008, **39**, 759–772.
41 L. M. Marcell and G. A. Beattie, *Molecular plant-microbe interactions*, 2002, **15**, 1236–1244.
42 N. Suvindran, F. Li, Y. Pan and X. Zhao, *Advanced Materials Interfaces*, 2018, **5**, 1800723.
43 S. Yang, J. Ju, Y. Qiu, Y. He, X. Wang, S. Dou, K. Liu and L. Jiang, *Small*, 2014, **10**, 294–299.